Applied Catalysis B: Environmental 140–141 (2013) 164–168

Contents lists available at SciVerse ScienceDirect

Applied Catalysis B: Environmental

journal homepage: www.elsevier.com/locate/apcatb

Red phosphor/g-C_3N_4 heterojunction with enhanced photocatalytic activities for solar fuels production

Yu-Peng Yuan[a,b], Shao-Wen Cao[a], Yu-Sen Liao[a], Li-Sha Yin[a], Can Xue[a,*]

[a] Solar Fuels Lab, School of Materials Science and Engineering, Nanyang Technological University, 50 Nanyang Avenue, Singapore 639798, Singapore
[b] Laboratory of Advanced Porous Materials, School of Chemistry and Chemical Engineering, Anhui University, Hefei 230039, PR China

ARTICLE INFO

Article history:
Received 23 January 2013
Received in revised form 26 March 2013
Accepted 1 April 2013
Available online 8 April 2013

Keywords:
Photocatalysis
H_2 production
CO_2 conversion
Heterostructure
Carbon nitride

ABSTRACT

We report a composite photocatalyst by coupling red phosphor (r-P) and graphitic carbon nitride (g-C_3N_4). The introduction of g-C_3N_4 onto r-P surface led to considerable improvement on the photocatalytic activity for H_2 production and CO_2 conversion into valuable hydrocarbon fuel (CH_4) in the presence of water vapor. The enhancement could be attributed to the effective separation of photogenerated electrons and holes across the r-P/g-C_3N_4 heterojunction. Owing to the advantages of non-toxicity, low cost and abundance in nature, this active heterostructural r-P/g-C_3N_4 photocatalyst would have great potential for efficient solar fuels production.

© 2013 Elsevier B.V. All rights reserved.

1. Introduction

Solar fuels have been considered as one of the most important renewable clean energy resources in the future. In the past decade, it has attracted tremendous efforts on developing various photocatalysts to generate chemical fuels through solar water splitting or CO_2 reduction [1–5]. Researchers have recognized that a single-component semiconductor photocatalyst is hardly competent for efficient solar fuels generation due to the problems of limited visible-light harvesting, rapid charge recombination, and poor stabilities [1–3]. Therefore, recently more and more attentions have focused on multi-component photocatalysts consisting of different semiconductor nanostructures, such as CdS/TiO_2 and p-$CaFe_2O_4$/n-$PbBi_2Nb_{0.9}W_{0.1}O_9$ photocatalytic nanodiode [6–8], in which the created heterojunctions can significantly improve the photogenerated charge separation and thereby promote the photocatalytic efficiency. Nevertheless, these hybrid photocatalysts involve at least one metal-containing semiconductor as a major component that would raise economic cost concern in terms of large-scale production.

Herein, we report a new hybrid photocatalyst made by coupling red phosphor (r-P) with graphitic carbon nitride (g-C_3N_4), referred as PCN-*x* (*x* is the mass percentage of g-C_3N_4 in the hybrid). Both components in this hybrid photocatalyst are composed by inexpensive earth-abundant elements, and exhibit wide absorption range in the visible light [9–13]. Although their conduction band edges are capable of reducing water for H_2 evolution according to literatures, the individual use of either material showed limited photocatalytic efficiency because of the high recombination rate of photogenerated electrons and holes [11–17]. Significantly, we found that the prepared PCN-*x* hybrids exhibit remarkably enhanced H_2 evolution yield in visible-light-driven water reduction. Even more, such a combination leads to a surprising enhancement on the CH_4 production yield in photocatalytic CO_2 conversion. This discovery demonstrates the potential of using economic materials for efficient solar fuels production.

2. Experiments

2.1. Preparation of PCN-x hybrids

All of the reagents were used without further treatment. The g-C_3N_4 used in this study was prepared by heating urea (≥97.0%, Sigma–Aldrich) to 550 °C for 4 h in Ar atmosphere. Red phosphor/g-C_3N_4 hybrids (PCN-*x*) were prepared by annealing the mixture of red phosphor and g-C_3N_4 in inert atmosphere. In a typical process, an appropriate amount of g-C_3N_4 was mixed with r-P (≥97.0%, Sigma–Aldrich). The mixture was ground for 30 min in a mortar and transferred into an alumina crucible that was sealed with aluminium silicate. The crucible was calcined at 380 °C for 2 h in Ar atmosphere, and then cooled down to room temperature in Ar atmosphere. Pure red phosphor sample without mixing g-C_3N_4

* Corresponding author. Tel.: +65 67906180; fax: +65 67909081.
E-mail address: cxue@ntu.edu.sg (C. Xue).

0926-3373/$ – see front matter © 2013 Elsevier B.V. All rights reserved.
http://dx.doi.org/10.1016/j.apcatb.2013.04.006

was also treated under the identical condition for comparison purpose.

3. Characterizations

X-ray powder diffraction (XRD) data were collected on a Shimadzu XRD-6000 X-ray diffractometer using Cu Kα1 radiation at a scan rate of 1°/min. The acceleration voltage and the applied current were 40 kV and 40 mA, respectively. Morphologies and structure of PCN-*x* hybrids were observed by field emission scanning electron microscopy (SEM: JEOL JSM-7600F) and transmission electron microscopy (TEM: JEOL JEM-2100F). TEM was operated at an accelerating voltage of 200 kV. UV–vis diffuse reflectance spectra (DRS) were recorded over the spectral range 320–800 nm on a Lambda 750 UV/vis/NIR spectrophotometer (Perkin Elmer, USA). $BaSO_4$ was used as a reflectance standard. The photoluminescence (PL) spectra were obtained on a Shimazu RF-5310PC fluorometer at an excitation wavelength of 350 nm. X-ray photoelectron spectra (XPS) of the as-prepared photocatalysts were recorded on a Thermo Scientific Theta Probe XPS using Al Kα radiation (1486.6 eV) and the binding energy values were calibrated with respect to C (1s) peak (284.6 eV). Fourier transform infrared spectra (FTIR) of the samples were recorded between 400 and 4000 cm^{-1} on an IRAffinity-1 FTIR spectrometer.

3.1. Photocatalytic hydrogen evolution

Photocatalytic H_2 production reactions were carried out in a 50-mL closed quartz flask reactor, which was sealed with Suba Seal rubber septa (Sigma–Aldrich). Typically, 10 mg of the prepared PCN-*x* hybrids were suspended in 10 mL aqueous solution of L-ascorbic acid (0.1 M, pH 4.0). A small amount of H_2PtCl_6 solution (61 μL, 0.08 wt%) was injected into the reactor to load 0.5 wt % Pt as co-catalyst on PCN-*x* surfaces through photodeposition. The reactor was purged with argon to drive away the residual air. The photocatalytic hydrogen evolution was initiated by irradiating the suspension with a 300-W xenon lamp (MAX-302, Asahi Spectra, USA) coupled with a UV cut-off filter (λ > 420 nm). The gas product was analyzed periodically through a gas chromatograph (GC-7890A, Agilent) with a TCD detector.

3.2. Photocatalytic conversion of CO_2 into CH_4

The photocatalytic CO_2 reduction was performed in a 100 mL gastight reactor with a quartz window and two side-sampling ports. In a typical process, 0.5 wt% Pt loaded PCN-*x* hybrids (20 mg) were dispersed on a 4-cm^2 glass substrate. The glass with powder photocatalysts was then put into the reactor. Prior to the irradiation, the reaction system was purged with high purity CO_2 for 30 min to remove the residual air and 0.2 ml ultrapure water was injected into the reaction system. A 500-W xenon arc lamp was used as the light source for the photocatalytic reaction. During the reaction, the gas product was analyzed periodically through a gas chromatograph (GC-7890A, Agilent) with a TCD detector.

4. Results and discussion

4.1. Sample characterizations

The PCN-*x* photocatalysts were prepared by annealing the mixture of red phosphor and g-C_3N_4 with different mass ratio in Ar atmosphere, as illustrated in Fig. 1A. PCN-5 and PCN-30 were used as representative samples for the studies. X-ray diffraction (XRD) patterns (Fig. 2) show no phase changes of both r-P and g-C_3N_4, and no sign of new product formation during the annealing process. The characteristic peak at 27.4° as the signature of interlayer aromatic packing indicates that the crystal structure of C_3N_4 was retained after the thermal treatment [11]. The FT-IR analyses (Fig. S1) further confirm that the original graphitic C–N backbones keep unchanged after hybridization with r-P, and show no vibrational peak of P-related groups in the PCN-*x* hybrids, indicating that the annealing process unlikely initiates new chemical bonding between r-P and g-C_3N_4. The UV–vis spectra (Fig. 3) of the PCN-*x* hybrids exhibit mixed absorption features of r-P and g-C_3N_4 [9,11]. As expected, r-P and g-C_3N_4 show their fundamental absorption edge at 700 nm and 460 nm, respectively. The absorption edge of g-C_3N_4 becomes more evident with the increase of g-C_3N_4 content in PCN-*x* hybrids.

Scanning electron microscopy (SEM) analyses (Fig. 1) reveal that in the PCN-5 hybrid, large g-C_3N_4 nanosheets with thickness of several tens nanometers are coating on the surface of r-P particles, while pure r-P particles show quite smooth and clean surfaces. The g-C_3N_4 layer was confirmed by energy-dispersive X-ray spectroscopy (EDS) as shown in Fig. S2. Increasing the g-C_3N_4 ratio leads to heavier g-C_3N_4 coverage over the r-P surfaces (Fig. 1D). Notably, g-C_3N_4 preferably coats on the uneven r-P surface area as evidenced by the less g-C_3N_4 coating on the very smooth area of r-P surfaces (Fig. S3, indicated by arrow 1) with some free g-C_3N_4 particles inevitably existing (Fig. S3, inicated by arrow 2).

This heavy g-C_3N_4 coating was hardly visualized in transmission electron microscopy (TEM), nevertheless, we still can observe g-C_3N_4 nanosheets adhering on the r-P edges as shown in Fig. 4. However, high-resolution TEM images of the samples are not attainable because these g-C_3N_4 nanosheet structures seem too thin and tend to transform into spherical structures under high energy focusing electron beam (Fig. S4). Note that upon thermal treatment (380 °C for 2 h), the pure g-C_3N_4 appears as velvet-like sheets with rolling edges (Fig. S5). Such flexible structures allow g-C_3N_4 anchoring on the r-P surfaces and in particular wrapping on the r-P edges, which creates heterojunctions between r-P and g-C_3N_4 for charge transfer [18].

4.2. Photocatalytic H_2 evolution

In order to identify the contribution of these heterojunctions, we have compared these samples for visible-light-driven (λ > 420 nm) photocatalytic H_2 generation from water reduction. Ascorbic acid (0.1 M) was used as sacrificial reagent, and Pt (0.5 wt%) were loaded as co-catalyst on the samples via in situ photodeposition [19]. Control experiments confirm no H_2 evolution without photocatalysts or light illumination. As illustrated in Fig. 5A, the pure r-P sample showed very weak activity for H_2 production (22 $\mu mol\ h^{-1}\ g^{-1}$). However, upon loading of 5 wt% g-C_3N_4 (as PCN-5) onto r-P surfaces, the H_2 evolution rate (310 $\mu mol\ h^{-1}\ g^{-1}$) was enhanced more than ten times and even comparable to that of pure g-C_3N_4 (340 $\mu mol\ h^{-1}\ g^{-1}$). In comparison, a simple mixture of r-P with 5 wt% g-C_3N_4 only showed a H_2 evolution rate of 70 $\mu mol\ h^{-1}\ g^{-1}$. These results demonstrate that thermal annealing facilitates the formation of r-P/g-C_3N_4 heterojunctions for effective charge separation in PCN-5, thereby leading to this enhanced H_2 evolution rate (more than 4 times enhancement by annealing). The photocatalytic activity can be further enhanced (up to 1000 $\mu mol\ h^{-1}\ g^{-1}$ for H_2 evolution) by increasing g-C_3N_4 content to 30 wt% (PCN-30). The above results clearly demonstrate that the r-P/g-C_3N_4 interface plays an essential role on enhancing photocatalytic H_2 evolution. Higher g-C_3N_4 loading on r-P leads to larger interfaces and thereby effective separation of photogenerated electrons and holes towards enhanced photocatalytic activities [20–22].

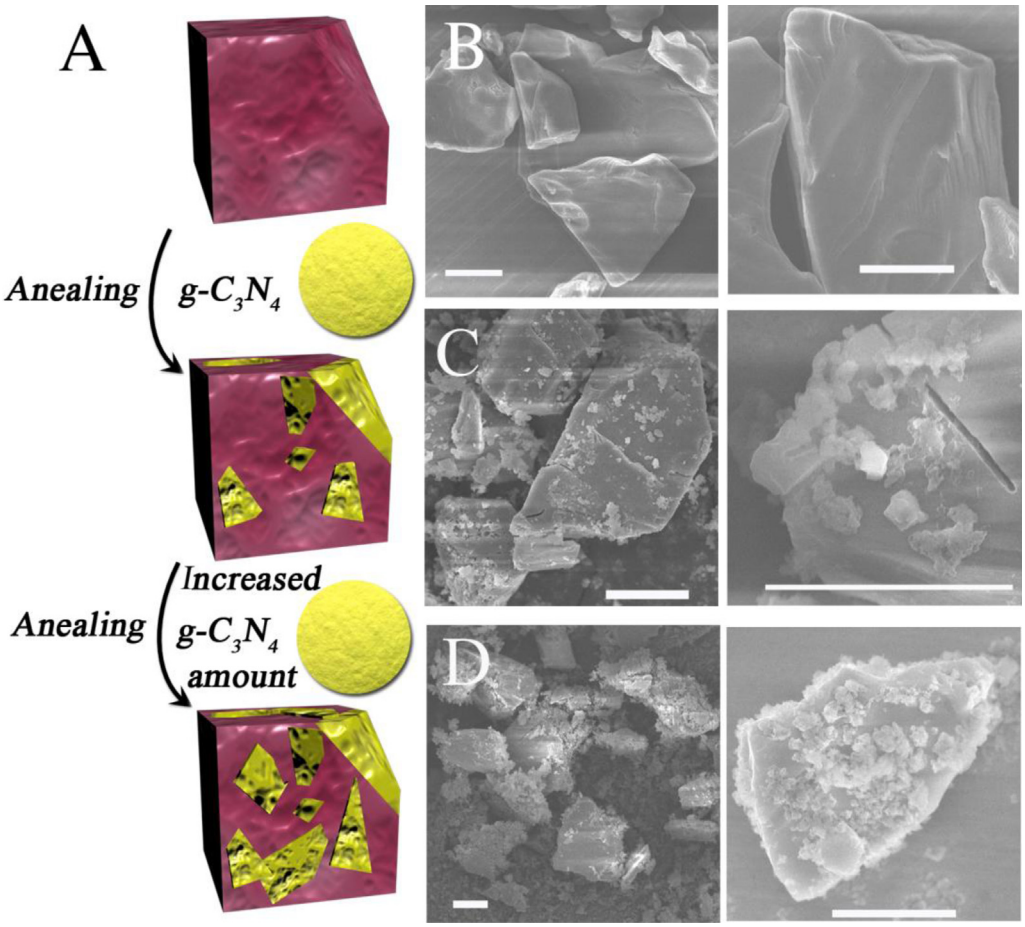

Fig. 1. (A) schematic illustration of attaching g-C_3N_4 on r-P surfaces via annealing. Increasing the g-C_3N_4 mass ratio leads to higher surface coverage of g-C_3N_4 on r-P surfaces. (B)–(D) SEM images of r-P, PCN-5, and PCN-30. The right column shows the magnified images of r-P, PCN-5, and PCN-30, respectively. Scale bar: 10 μm.

4.3. Photocatalytic CO_2 conversion

Furthermore, since the reduction potential from CO_2 to CH_4 ($CO_2 + 8H^+ + 8e^- \rightarrow CH_4 + 2H_2O$) is around −0.24 V, the high conduction band (CB) edge of r-P (−0.25 V vs. NHE) and g-C_3N_4 (−1.2 V vs. NHE) allows us to use the PCN hybrids for photocatalytic conversion of CO_2 into hydrocarbon fuels [9,11,23–25]. As shown in Fig. 5B, the PCN-30 exhibited a CH_4 production yield of 295 μmol h^{-1} g^{-1}, which is twice higher than pure r-P (145 μmol h^{-1} g^{-1}) and nearly three times higher than pure g-C_3N_4 (107 μmol h^{-1} g^{-1}). This comparison results further demonstrate that the coupling between r-P and g-C_3N_4 effectively promote the overall photocatalytic activity for CO_2 reduction.

4.4. Mechanism of enhanced photocatalytic activity

The enhanced photocatalytic activity could be attributed to the effective interfacial charge transfer between r-P and g-C_3N_4 across the heterojunction as illustrated in Fig. 6. Since the CB edge of g-C_3N_4 (−1.2 V vs. NHE) is more negative than that of r-P (−0.25 V vs.

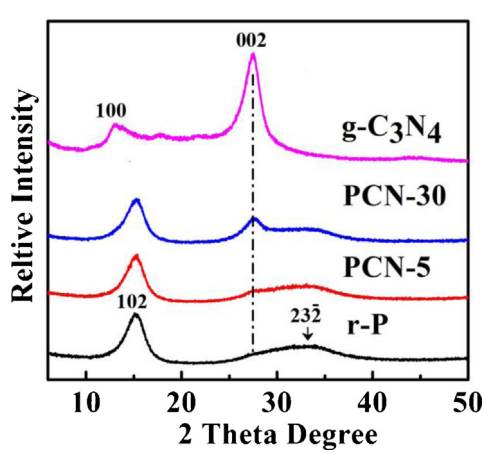

Fig. 2. XRD patterns of PCN-*x* hybrids. The XRD patterns of pure g-C_3N_4 and r-P that were treated at 380 °C for 2 h were also provided for comparison.

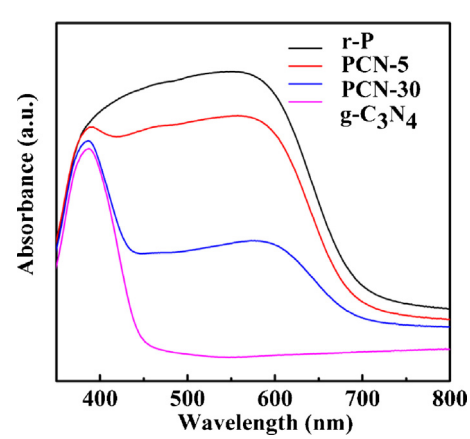

Fig. 3. UV–vis absorption spectra of PCN-5, PCN-30, g-C_3N_4 and r-P sample.

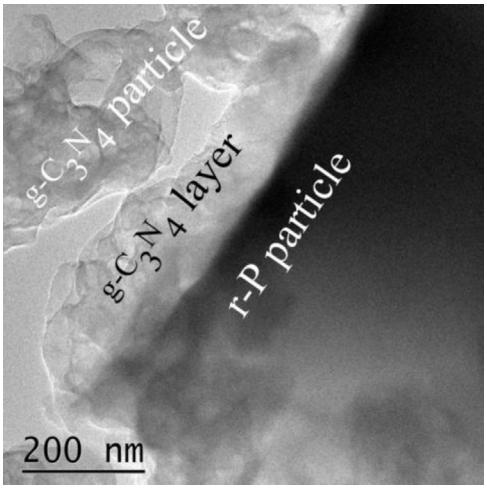

Fig. 4. TEM image of PCN-30. The covered g-C_3N_4 layer on r-P surfaces and linked g-C_3N_4 particle are labeled.

NHE), the photoexcited electrons on g-C_3N_4 surface could transfer to r-P through the interfaces created by annealing. Similarly, the photoinduced holes on the r-P surface move towards g-C_3N_4 due to the difference in valence band (VB) edge potentials. The accumulated electrons on r-P surfaces reduce the H^+ or CO_2 into valuable fuels, while the holes on g-C_3N_4 surfaces oxidize the electron donor (ascorbic acid for H_2 production and OH^- for CO_2 reduction, respectively). The effective separation of photogenerated electrons and holes thus enhances the photocatalytic activities [21,22]. In addition, the network structure of g-C_3N_4 can acts as an excellent

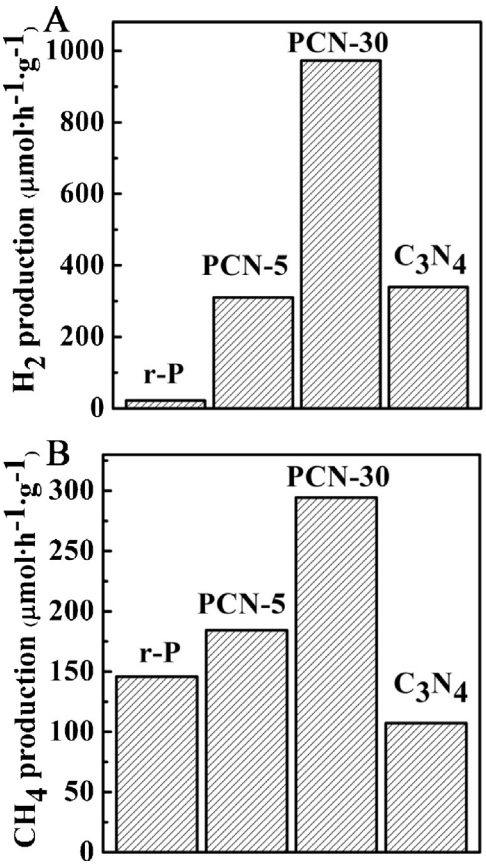

Fig. 5. Photocatalytic (A) H_2 and (B) CH_4 production rate of r-P, PCN-5, PCN-30, and g-C_3N_4 photocatalysts.

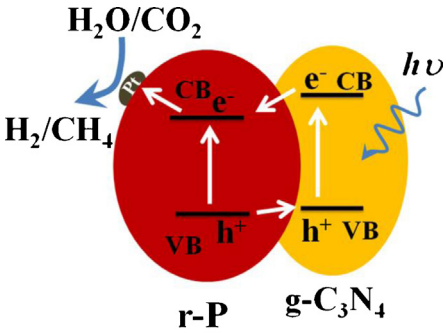

Fig. 6. Energy band diagram of PCN-*x* under zero bias and schematic illustration of electron–hole separation process after excitation.

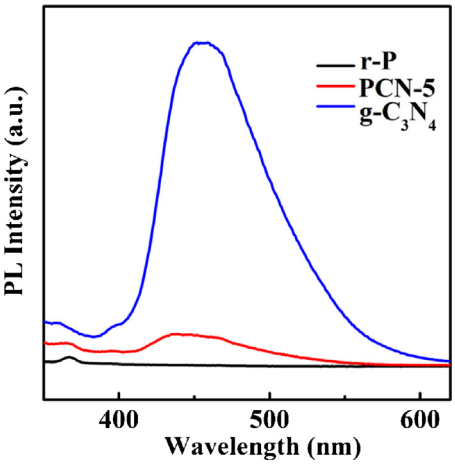

Fig. 7. Photoluminescence spectra of r-P, PCN-5 and g-C_3N_4 at an excitation wavelength of 350 nm.

electron transport platform to facilitate the charge transfer process [17,18].

The interfacial charge transfer could be also evidenced by the decreased photoluminescence (PL) intensity in the PCN-5 hybrid (Fig. 7) as compared to pure g-C_3N_4. This result further confirms photoinduced electron flowing direction from g-C_3N_4 to r-P, causing PL quenching of g-C_3N_4 in PCN-5. Meanwhile, the interfacial charge transfer could be further supported by the enhanced TAOH fluorescence intensity on PCN-5 as compared to that on pure g-C_3N_4 (Fig. S6, see supporting informatio for details). This observation also indicated that the r-P/g-C_3N_4 heterojunctions allow the photocatalyst to supply more photogenerated holes to generate more ·OH radicals and thus higher TAOH concentration with stronger fluorescence signal.

In addition, X-ray photoelectron spectroscopy (XPS) analyses reveal that the annealing process neither creates new species such as P_3N_5 nor leads to P-doping into the g-C_3N_4 lattice (P_3N_5 is a very stable species) [26]. As shown in Fig. S7, the P 2p signal can be deconvoluted into ~129.3 eV and ~130.1 eV for P $2p_{3/2}$ and P $2p_{1/2}$, respectively, which are the typical signatures for 2p binding energy of red phosphor. No binding energy shift is observed for PCN-30 as compared to pure r-P, indicating no P-N bonding formation.

5. Conclusions

In summary, hybrid structures of r-P and g-C_3N_4 are prepared through solid state annealing method. We found that small amount introduction of g-C_3N_4 onto r-P surface led to considerable improvement on the photocatalytic activity for H_2 production and CO_2 conversion into CH_4. The enhancement could be attributed

to the effective separation of photogenerated electrons and holes across the r-P/g-C_3N_4 heterojunction. This work provides a new insight on developing active metal-free heterostructural photocatalysts and demonstrates the great potential of using economic materials for efficient solar fuels production.

Acknowledgements

This work is financially supported by NTU Start-Up Grant (SUG), NTU seed funding for Solar Fuels Laboratory, MOE AcRF-Tier1 RG 44/11, MOE AcRF-Tier 2 (MOE2012-T2-2-041, ARC 5/13), and CRP (NRF-CRP5-2009-04) from NRF Singapore. Y. P. Yuan acknowledges the support from the National Natural Science Foundation of China (No. 51002001).

Appendix A. Supplementary data

Supplementary data associated with this article can be found, in the online version, at http://dx.doi.org/10.1016/j.apcatb.2013.04.006.

References

[1] X.B. Chen, S.H. Shen, L.J. Guo, S.S. Mao, Chemical Reviews 110 (2010) 6503–6570.
[2] H. Tong, S.X. Ouyang, Y.P. Bi, N. Umezawa, M. Oshikiri, J.H. Ye, Advanced Materials 24 (2011) 229–251.
[3] A. Kudo, Y. Miseki, Chemical Society Reviews 38 (2009) 253–278.
[4] L. Ge, C.C. Han, Applied Catalysis B: Environmental 117–118 (2012) 268–274.
[5] S.C. Roy, O.K. Varghese, M. Paulose, C.A. Grimes, ACS Nano 4 (2010) 1259–1278.
[6] H. Tada, T. Mitsui, T. Kiyonaga, T. Akita, K. Tanaka, Nature Materials 5 (2006) 782–786.
[7] D.R. Baker, P.V. Kamat, Advanced Functional Materials 19 (2009) 805–811.
[8] H.G. Kim, P.H. Borse, W. Choi, J.S. Lee, Angewandte Chemie International Edition 44 (2005) 4585–4589.
[9] F. Wang, W.K.H. Ng, J.C. Yu, H.J. Zhu, C.H. Li, L. Zhang, Z.F. Liu, Q. Li, Applied Catalysis B: Environmental 111–112 (2012) 409–414.
[10] F. Wang, C.H. Li, Y.C. Li, J.C. Yu, Applied Catalysis B: Environmental 119–120 (2012) 267–272.
[11] X.C. Wang, K. Maeda, A. Thomas, K. Takanabe, G. Xin, J.M. Carlsson, K. Domen, M. Antonietti, Nature Materials 8 (2009) 76–80.
[12] Y. Zheng, J. Liu, J. Liang, M. Jaroniec, S.Z. Qiao, Energy & Environmental Science 5 (2012) 6717–6731.
[13] Y.J. Zhang, A. Thomas, M. Antonietti, X.C. Wang, Journal of the American Chemical Society 131 (2009) 50–51.
[14] Y.J. Zhang, T. Mori, J.H. Ye, M. Antonietti, Journal of the American Chemical Society 132 (2010) 6294–6295.
[15] Y. Wang, X.C. Wang, M. Antonietti, Angewandte Chemie International Edition 51 (2012) 68–89.
[16] S.C. Yan, Z.S. Li, Z.G. Zou, Langmuir 26 (2010) 3894–3901.
[17] C.S. Pan, J. Xu, Y.J. Wang, D. Li, Y.F. Zhu, Advanced Functional Materials 22 (2012) 1518–1524.
[18] Y.J. Wang, R. Shi, J. Lin, Y.F. Zhu, Energy & Environmental Science 4 (2011) 2922–2929.
[19] S.W. Cao, Z. Yin, J. Barber, F.Y.C. Boey, S.C.J. Loo, C. Xue, ACS Applied Materials & Interfaces 4 (2012) 418–423.
[20] X.X. Xu, G. Liu, C. Randorn, J.T.S. Irvine, International Journal of Hydrogen Energy 36 (2011) 13501–13507.
[21] J.X. Sun, Y.P. Yuan, L.G. Qiu, X. Jiang, A.J. Xie, Y.H. Shen, J.F. Zhu, Dalton Transactions 41 (2012) 6756–6763.
[22] S.C. Yan, S.B. Lv, Z.S. Li, Z.G. Zou, Dalton Transactions 39 (2010) 1488–1491.
[23] Y.J. Zhang, M. Antonietti, Asian Journal of Chemistry 5 (2010) 1307–1311.
[24] Q. Liu, Y. Zhou, J.H. Kou, X.Y. Chen, Z.P. Tian, J. Gao, S.C. Yan, Z.G. Zou, Journal of the American Chemical Society 132 (2010) 14385–14387.
[25] G.H. Dong, K. Zhao, L.Z. Zhang, Chemical Communications 48 (2012) 6178–6180.
[26] K. Landskron, H. Huppertz, J. Senker, W. Schnick, Angewandte Chemie International Edition 40 (2001) 2643–2645.